Journal of Magnetic Resonance Open 12-13 (2022) 100067

Contents lists available at ScienceDirect

Journal of Magnetic Resonance Open

journal homepage: www.sciencedirect.com/journal/journal-of-magnetic-resonance-open

Analysis and information content of quadrupolar NMR in glasses: ^{25}Mg NMR in vitreous $MgSiO_3$ and $CaMgSi_2O_6$

Marcos de Oliveira Jr. [a,*], Hugo Damasceno [a], Philip S. Salmon [b], Hellmut Eckert [a,c,**]

[a] Instituto de Física de São Carlos, Universidade de São Paulo, Avenida Trabalhador Sãocarlense 400, São Carlos, SP 13566-590, Brazil
[b] Department of Physics, University of Bath, Bath BA2 7AY, United Kingdom
[c] Institut für Physikalische Chemie, WWU Münster, Corrensstraße 30, D 48149 Münster, Germany

ARTICLE INFO

Keywords:
25Mg solid state NMR
25Mg-enriched glasses
Enstatite
Diopside
Glasses

ABSTRACT

The static wideline and high-resolution magic angle spinning (MAS) ^{25}Mg NMR lineshapes measured for isotopically enriched enstatite and diopside glasses indicate a wide distribution of the electric-field gradient (EFG) components at the ^{25}Mg position caused by disorder. The correct characterization of this distribution requires simulations with special attention paid to the experimental parameters. Here, both the static spectra obtained by wideband excitation and the MAS-NMR spectra obtained via rotor-synchronized Hahn spin echo acquisition were successfully simulated with the Czjzek distribution model, using one consistent set of parameters. Average nuclear electric quadrupole coupling constants near 8 MHz and a distribution width around 4 MHz were obtained for both materials, which suggests that earlier results on these glasses need to be re-examined. The results of this study outline a general strategy for characterizing the local environments of strongly coupled quadrupolar nuclei in amorphous and glassy materials. Despite the discrepancies between the interaction parameters extracted from our data and those published in earlier NMR work, the best fit to the data indicate an average isotropic chemical shift near 13 ppm (vs. aqueous $MgCl_2$ solution) for both the enstatite and diopside glasses. Assuming the applicability of the current database relating the ^{25}Mg chemical shifts with coordination numbers in crystalline compounds, this value suggests that the Mg^{2+} ions are six-coordinated. This conclusion, however, is based on the simplifying assumption that the ^{25}Mg spectrum comprises a Czjzek distribution centered at a single isotropic chemical shift value and stands in contrast to the results of recent isotope-selective neutron diffraction studies which give an average Mg-O coordination number of 4.4–4.5 for both glasses. However, reasonable fits to the MAS-NMR spectra can also be obtained when constraining the average isotropic chemical shift to 50 ppm, a value typical of four-coordinated Mg. We conclude that multiple Mg sites with different coordination numbers may well be present and that, in the present glasses, ^{25}Mg NMR at typically used spinning rates and magnetic field strengths (20 kHz, 14.1 T) is not capable of resolving them due to excessive broadening by quadrupolar interactions.

Introduction

Magnesium is a key element in the solid-state science of many technologically important materials [1–4]. In the design of mechanically strong and chemically resistant oxide glasses, it is known to be a valuable additive for enhancing their mechanical stability and for overcoming conflicting constraints for designing glasses with high elastic moduli and high crack initiation resistance [2,3]. In the area of bioactive glasses, magnesium is also an important additive, modifying their dissolution kinetics and apatite mineralization properties [5–8]. The structural role of Mg in glassy materials is, however, the subject of considerable uncertainty and controversy, as experimental results addressing this question have been interpreted in rather contradictory ways. While some authors consider Mg as a regular network modifier [5], other studies have suggested it to be integrated into the network as doubly charged four-coordinated MgO_4^{2-} species [6]. Its coordination number in silicate glasses is a matter of on-going debate, where values of four [9], four-to-five [10–12] and six [13–15] have been proposed. In general, diffraction results and molecular dynamics simulations favor lower coordination numbers [10,16–22], whereas the chemical shifts

* Corresponding author.
** Corresponding author.
E-mail addresses: mjunior@ifsc.usp.br (M. de Oliveira), eckert@ifsc.usp.br (H. Eckert).

https://doi.org/10.1016/j.jmro.2022.100067
Received 14 June 2022; Received in revised form 26 July 2022; Accepted 9 August 2022
Available online 10 August 2022

δ_{iso} obtained from solid-state nuclear magnetic resonance (NMR) experiments tend to support higher coordination numbers [13–15,23,24]. Recent work by Bisbrouck et al. [25] has suggested that the presence of sodium in silicate glasses may stabilize Mg with lower coordination numbers.

As discussed in the literature, solid state NMR studies addressing the local coordination environment of magnesium are seriously handicapped by the low magnetic moment (the gyromagnetic ratio amounts to 1.639×10^7 rad T^{-1} s^{-1}) and the relatively low natural abundance (10%) of the only NMR active isotope, which is ^{25}Mg. At 14.1 T, the resonance frequency is 36.7 MHz for samples with a cubic local environment. If the environment is non-cubic, the sizeable quadrupole moment of the ^{25}Mg nuclide interacts with the local electric field gradients (EFGs), producing anisotropic resonance frequency distributions that can be theoretically predicted by second-order perturbation theory. In this way, the Hamiltonian interaction parameters for many crystalline compounds have been analyzed [26–36], leading to results in good agreement with ab-initio calculations [26,27,29]. Such work has suggested that the ^{25}Mg isotropic chemical shifts should be able to differentiate between Mg species in four- versus six-coordination: most six-coordinated Mg compounds yield δ_{iso} values between zero and 30 ppm relative to aqueous $MgCl_2$ solution (with some negative shifts observed in phosphates), while the chemical shifts of åkermanite, spinel, and various other minerals featuring four-coordinated Mg are found within the range 40–80 ppm [34].

On the other hand, George and Stebbins [37] have reported high temperature (1000 – 1470 °C) ^{25}Mg NMR results on several magnesium silicate and aluminosilicate melts. Due to the fast isotropic motion in the liquid state, the second-order quadrupolar effect is averaged out, resulting in isotropic spectra [37]. A single-line spectrum for the $CaMgSi_2O_6$ melt with an isotropic chemical shift of 22 ppm was reported, which reflects a time-averaged value over all coordination states. At the present stage, inferences about the Mg coordination number from ^{25}Mg isotropic chemical shifts in glasses and melts are still uncertain because of the limited database on fourfold and fivefold coordinated crystalline reference compounds. Furthermore, the situation in the melt (with fluctuating Mg-O and Si-O chemical bonds) does not necessarily reflect the disorder associated with the glass structure.

A serious complication in applying these results to the structural analysis of magnesium in vitreous materials arises from the fact that the EFGs in glass appear to have a very wide distribution. This distribution is indicated by molecular dynamics simulations, which reveal a wide range of local geometries for the Mg^{2+} coordination environment [20,22]. Therefore, the ^{25}Mg magic angle spinning (MAS) NMR spectra for glasses measured at moderate magnetic field strengths (such as 14.1 T) are broadened, which prevents the spectral resolution of resonances from multiple Mg^{2+} sites. It is also possible that a proportion of the ^{25}Mg nuclei are not detected under MAS conditions due to extremely strong quadrupolar interactions, as recently shown for the distorted Mg(2) site in orthoenstatite [29]. Ultimately, this complication makes the precise measurement of isotropic chemical shifts (and hence an assignment of the coordination number) rather difficult due to the lack of site resolution, even under fast MAS conditions.

In the present contribution, we have studied this issue by a more detailed analysis of the effects of EFG distributions upon the static and MAS-NMR spectra of vitreous $MgSiO_3$ (enstatite) and $CaMgSi_2O_6$ (diopside) by turning to isotopically enriched glasses, prepared from isotopically pure ^{25}MgO. Relative to a sample containing an identical amount of magnesium of natural isotopic abundance, the tenfold increase in ^{25}Mg content is expected to produce a 100-fold reduction in the number of accumulated free induction decays for reaching a comparable signal-to-noise ratio. Here we report the results of a preliminary study of static wideline and high-resolution ^{25}Mg NMR lineshapes, including the measurement of the quadrupolar satellite transitions using wideband excitation techniques. Furthermore, we examine the potential of spin echo decay spectroscopy to measure ^{25}Mg-^{25}Mg magnetic dipole-dipole couplings. The results give new insight into the informational content of ^{25}Mg NMR in revealing the structural properties of magnesium in silicate glasses.

Experimental

Sample preparation and characterization

The enstatite composition glass $MgSiO_3$ was made using the procedure described in Ref. [21] from ^{25}MgO (98.49%), containing residuals of 1.00% ^{24}Mg and 0.51% ^{26}Mg, and SiO_2 (> 99%). The dried chemicals were ground together and melted in air at 1650 °C in a Pt-10% Rh crucible. The melt was quenched by immersing the bottom of the crucible in water. The sample was then ground and remelted twice to ensure a homogeneous glass. The sample composition measured by electron probe microanalysis was 49.16(5) mol% MgO and 50.84(5) mol % SiO_2. The diopside composition glass $CaMgSi_2O_6$ was made using the procedure described in Ref. [38] from ^{25}MgO (98.79%), containing residuals of 0.81% ^{24}Mg and 0.40% ^{26}Mg, $CaCO_3$ (> 99%) and SiO_2 (> 99%). The starting chemicals were decarbonised overnight at 800 °C and melted in air at ~1492 °C in a Pt-10%Rh crucible. The melt was quenched by immersing the bottom of the crucible in water. The melting procedure was then repeated to ensure a homogeneous glass.

Solid-state NMR

Solid-state NMR studies were carried out at room temperature at magnetic flux densities of 5.64 and 14.1 T, using an Agilent DD2 console and a Bruker Avance Neo 600 MHz spectrometer, respectively. ^{29}Si MAS-NMR spectra were recorded on the Agilent DD2 spectrometer, at 5.64 T, using 4.0 mm rotors spun at a frequency of 5000 Hz, using 90° pulses of 4 μs length and a relaxation delay of 900 s. Spectra were simulated assuming Gaussian lineshapes. ^{25}Mg MAS-NMR spectra were obtained at 36.8 MHz (14.1 T) in the form of rotor-synchronized Hahn spin echoes on the Bruker Avance Neo 600 spectrometer, using 3.2 mm rotors spun at a rate of 20.0 kHz. Experiments were performed at two different power levels corresponding to non-selective nutation frequencies ν_1 of 25 and 80 kHz (measured on cubic MgO). The effective 90° pulse lengths were optimized by maximizing the echo intensity in a $t_p - \tau - 2t_p - \tau - acq$ scheme, with t_p values of 9 and 3.5 μs, respectively, for the two nutation frequencies employed. The τ values where chosen as 50 μs A relaxation delay of 0.5 s was used. Static spectra were measured using a Wideband Uniform Rate Smooth Truncation (WURST) pulse sequence [39–44] combined with the Carr-Purcell-Meiboom-Gill (CPMG) echo train acquisition scheme [45,46]. Compared to conventional CPMG experiments, WURST-CPMG experiments have the advantage of exciting nuclei over a wider frequency range, owing to the frequency variations of the pulses employed, thereby reducing the need for frequency stepping [42]. To cover a wider frequency range, signal acquisition was nevertheless done at multiple distinct base frequencies, corresponding to resonance offsets of ±5000, ±10,000 ppm and up to ±30,000 ppm from the center of the central $m = 1/2 \leftrightarrow m = -1/2$ transition, where m denotes the magnetic quantum number. These spectra were recorded to examine whether the central transition suffered any lineshape distortion owing to the limited probe bandwidth, and with the objective of testing for the presence of non-central ($|m| = 1/2 \leftrightarrow |m| = 3/2$ and $|m| = 3/2 \leftrightarrow |m| = 5/2$) satellite transitions, which are affected to different extents by the anisotropy of the nuclear electric quadrupolar interactions. WURST experiments were performed using excitation and refocusing pulses with an identical length of 50.0 μs, the excitation bandwidth was set to 1 MHz, and a recycle delay of 0.2 s was used. Pulse spacing was adjusted to yield a spikelet separation of 6.7 kHz and the number of Meiboom−Gill loops was set to 256.

For displaying the WURST-CPMG spectra, we have performed a fast Fourier transform of the whole echo train, resulting in spikelet patterns tracing the envelope of the static lineshape. MAS lineshape simulations

were performed using the ssNake [47] software and static simulations were performed using a homebuilt Matlab® code which uses the SIMPSON [48] software as the kernel for spectral simulations.

^{25}Mg Hahn spin echo decays were recorded on non-spinning samples with and without isotopic enrichment to test the sensitivity of this method for measuring the strength of the ^{25}Mg-^{25}Mg magnetic dipole-dipole couplings. These measurements were carried out at two different radiofrequency power levels, corresponding to non-selective nutation frequencies (ν_1) of 25 kHz and 80 kHz.

Chemical shifts are reported relative to solid secondary standards of MgO with the natural isotope distribution [δ_{iso}(^{25}Mg) = 27 ppm vs. aqueous $MgCl_2$ solution], and kaolinite [δ_{iso}(^{29}Si) = −91.5 ppm vs. tetramethylsilane (TMS)].

Results and discussion

^{29}Si MAS-NMR spectra

Fig. 1 shows the ^{29}Si MAS NMR spectra of the ^{25}Mg enriched samples. Owing to the small amount of material available, the signal-to-noise ratio was severely limited. The situation is further aggravated by extremely long spin-lattice relaxation times. The spectra shown in Fig. 1 took typically 48 h to accumulate. Because of these limitations, a reliable signal deconvolution in terms of the contributions from the separate Q^n species, where n denotes the number of bridging oxygen atoms per SiO_4 tetrahedron, could not be obtained. The spectra are, however, consistent with previously published data [49–53] where the simulations generally assume a distribution of Q^1, Q^2, Q^3, and Q^4 environments [49–51]. The lineshape fitting model of this kind comes close to the concept of a statistical distribution of the non-bridging oxygen atoms over the various silicon atoms. Table 1 summarizes the lineshape fitting parameters. Within the experimental error, the quantitative area ratios of the different Q^n species are consistent with the non-bridging oxygen to silicon atom ratio ⟨NBO/Si⟩ = 2:1 of the glass formulation.

Static ^{25}Mg NMR spectra

Fig. 2 summarizes the static ^{25}Mg NMR spectra obtained via the WURST-CPMG pulse sequence measured at different resonance offsets. The spectra resemble those typically observed for quadrupolar nuclei subjected to strong EFGs, necessitating second-order perturbation theory for the lineshape description. In particular, the asymmetric lineshape illustrates the presence of a wide distribution of quadrupolar coupling strengths, reflecting the intrinsic disorder of the glassy state. When measured with different resonance offsets, the central transition lineshape reveals the expected distortions due to the limited probe bandwidth. However, the results suggest that these distortions can be considered negligible when the frequency carrier is positioned at the resonance maximum of the lineshape, where it can be modelled without having to consider off-resonance distortions.

Mathematically, these spectra can be modeled with the Czjzek distribution [54,55]. This distribution gives an estimate of the probability $P(C_Q, \eta)$ of finding local environments with particular values of the parameters C_Q and η that describe the strength and shape of the quadrupolar interaction tensor, respectively. It assumes that in the absence of disorder, the chemical environment of the nuclei is isotropically symmetric, i.e., the EFG is zero. Disorder is introduced by considering a normal statistical distribution for the EFG components. The Czjzek probability function is given by the following expression [54,55]:

$$P(C_Q,\eta) = \frac{1}{\sqrt{2\pi}\sigma^5} C_Q^4 \eta \left(1 - \frac{\eta^2}{9}\right) \exp\left[\frac{-C_Q^2\left(1+\frac{\eta^2}{3}\right)}{2\sigma^2}\right] \quad (1)$$

where σ is the width of the distribution.

Fig. 3 shows a simulation of the ^{25}Mg static spectra using the Czjzek model. The simulation is obtained from the weighted average [having $P(C_Q, \eta)$ as the weighting factor] of a series of quadrupolar powder patterns with C_Q and η in the ranges $0 < C_Q < 16$ MHz and $0 < \eta < 1$, respectively, and isotropic chemical shift tensors with fixed δ_{iso} values. Each individual powder spectrum was simulated using a full matrix calculation in SIMPSON [48] over 46,368 orientations in a so-called ZCW full sphere scheme [56]. As shown in Fig. 3, this model successfully reproduces the measured asymmetric lineshapes, using widths for the Czjzek distributions (σ) of 4.4 and 4.2 MHz, corresponding to average $<|C_Q|>$ values (defined in terms of the modulus) of 8.6 and 8.3 MHz for the $MgSiO_3$ and $CaMgSi_2O_6$ samples, respectively. For both materials the average isotropic chemical shift was estimated at 13 ppm. The optimization of the simulations in Fig. 3 was performed with the objective of finding a single set of parameters for each sample that reproduces both the static and the MAS spectra (shown in Fig. 5).

Fig. 4a shows the experimental and simulated static spectra over their full-scale range. Distinctive spikelet patterns are clearly visible to both sides of the central resonance, which can be attributed to the satellite transition manifold. Fig. 4b shows a vertical expansion of the scale, revealing that the experimentally observed satellite transition spikelets are reduced in intensity in comparison to the simulations using the Czjzek model. We suggest that this deviation between simulated and experimental spectra may arise from a less efficient excitation of satellite transitions by the WURST pulses.

^{25}Mg MAS NMR spectra

An analysis of the MAS-NMR lineshapes offers an alternative way of

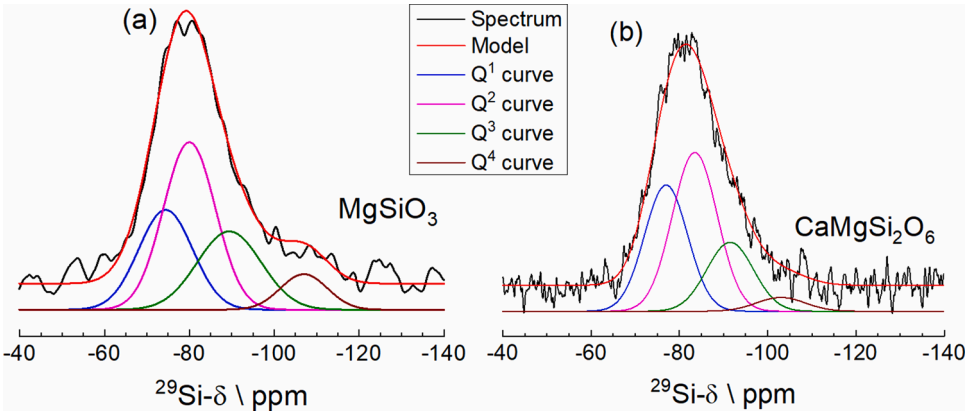

Fig. 1. ^{29}Si MAS-NMR spectra of (a) ^{25}Mg enriched enstatite glass and (b) ^{25}Mg enriched diopside glass (right). The red curve shows a lineshape simulation based on the fitting model of Ref. [49].

Table 1
Parameters (isotropic chemical shift δ_{iso}, full width at half maximum Δ, and fractional area in percent *I*) used in the deconvolution of the ^{29}Si MAS-NMR spectra (shown in Fig. 1) into the contributions from the individual Q^n components. ⟨NBO/Si⟩ denotes the average number of non-bridging oxygen atoms per silicon atom calculated from the quantitative Q^n distribution.

Sample	Parameters	Q^1	Q^2	Q^3	Q^4	$\langle\delta_{iso}\rangle$	⟨NBO/Si ⟩
$MgSiO_3$	δ_{iso}(± 1 ppm)	−74	−80	−89	−107	−83	1.86
	Δ (±1 ppm)	16	14	18	13		
	I (± 2%)	26	42	24	8		
$CaMgSi_2O_6$	δ_{iso}(± 1 ppm)	−78	−84	−93	−103	−84	2.05
	Δ (±1 ppm)	13	11	11	11		
	I (± 2%)	33	43	20	4		

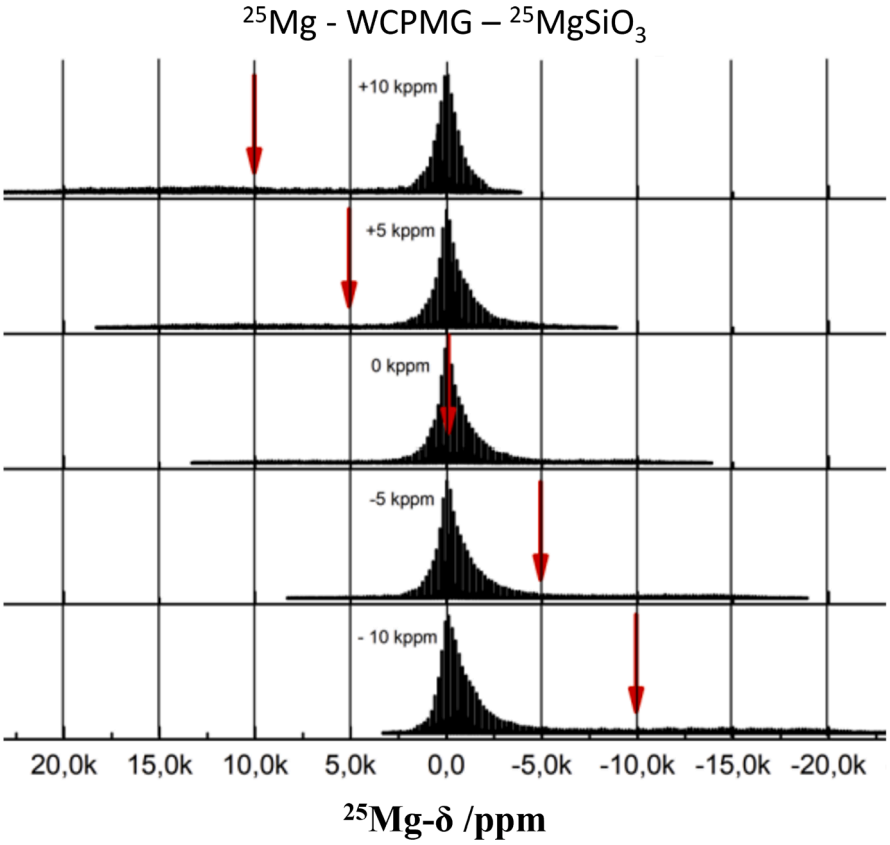

Fig. 2. Static ^{25}Mg WURST-CPMG spikelet spectra obtained on $MgSiO_3$ glass measured at different resonance offsets as marked by the red arrows.

obtaining the relevant internal interaction parameters affecting the Zeeman levels of the ^{25}Mg nuclei. Because of serious probe ringing problems at these rather low resonance frequencies, the best possible method for obtaining high-fidelity MAS-NMR lineshapes is the measurement of rotor-synchronized MAS echoes.

Fig. 5 shows the results obtained at two different power levels, corresponding to non-selective ^{25}Mg nutation frequencies (ν_1) of 25 and 80 kHz, respectively. The spectra obtained with a lower radiofrequency power level ($\nu_1 = 25$ kHz) are slightly narrower, which we relate to the well-known effect of the more limited excitation window available at lower radiofrequency power due to the use of longer pulse lengths. The MAS-NMR lineshapes of both glasses are very similar. We observe two distinct lineshape contributions: a broad, rather ill-defined feature covering a frequency region of ∼100 kHz and a narrower peak reflecting the effect of a distribution of quadrupolar coupling interactions in the regime of second-order perturbation theory that is frequently observed for other quadrupolar nuclei (^{23}Na, ^{27}Al) in glassy materials.

Fig. 5 shows that the entire lineshape can be successfully modelled using a Czjzek distribution, implemented within the ssNake program [47]. The simulations were performed assuming finite MAS, where 16 spinning side bands were simulated by the *Carousel* averaging approach implemented in the software. An unconstrained fitting approach was used to determine the best-fit parameters. The simulation parameters obtained for the high-power spectra reveal the existence of a wide distribution of quadrupolar coupling constants, σ, of 4.4 and 4.2 MHz, corresponding to average values $<|C_Q|>$ of 8.6 and 8.3 MHz for the $MgSiO_3$ and $CaMgSi_2O_6$ samples, respectively, and an average chemical shift of 13 ppm for both glasses. A Gaussian line-broadening of 27 ppm was included in the fit to account for a distribution of isotropic chemical shifts. Note that the MAS-fits shown in Fig. 5 use the same parameters as the fits to the static spectra, adding confidence to the analysis presented here. On the other hand, the width σ of the Czjzek distribution is slightly underestimated by fitting the same model to the low-power spectra, with σ values of 4.1 and 3.7 MHz for the $MgSiO_3$ and $CaMgSi_2O_6$ glasses, respectively.

We have also investigated the same NMR signals by employing a commonly used practice to analyze partially narrowed spectra by removing the broader parts of the lineshape by doing some left shifting on the time domain signal, effectively limiting the Czjzek analysis to the narrower feature. As shown in Fig. 6a, apparently satisfactory fits can be

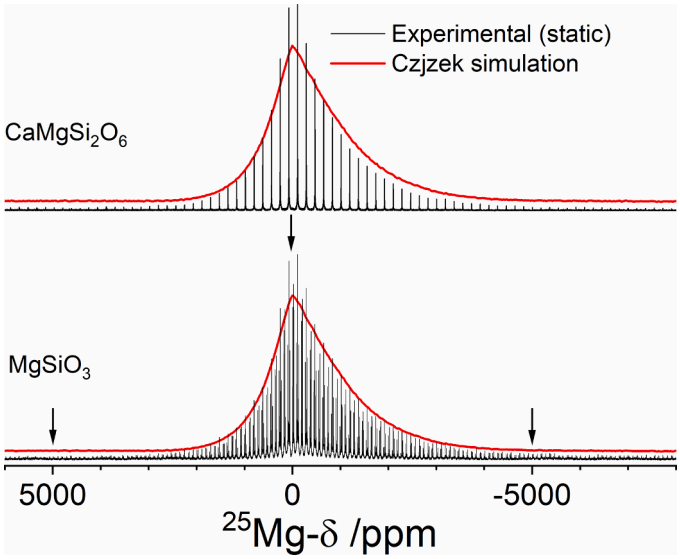

Fig. 3. Static ^{25}Mg WURST-CPMG spikelet spectra for both samples ($MgSiO_3$ and $CaMgSi_2O_6$) and the Czjzek distribution simulations obtained by fixing the parameters obtained from the simulations of high-power MAS fittings (Fig. 5). The arrows indicate the resonance offsets used for the stepwise acquisition of the wideline spectra.

obtained by this procedure for both the glasses considered here, even though it leads to an artificially reduced σ value of 2.8 MHz for both materials. In consequence, the average value $<|C_Q|>$ of 5.6 MHz for both glasses is significantly lower than the values obtained in the full analysis, and the apparent isotropic chemical shifts are also changed to 26 and 33 ppm for the $MgSiO_3$ and $CaMgSi_2O_6$ glasses, respectively. We note that a similar systematic error may occur if the spectra of glasses are measured via single-pulse acquisition in samples with the natural isotopic abundance of magnesium. Here, some left-shifting is often practiced in order to eliminate the effects of pulse breakthrough and acoustic ringing, leading to an artificial flattening of the baseline following a first-order phase correction.

To estimate the error associated with this spectral manipulation, Fig. 6b shows the result of the Czjzek model fitting analysis for data obtained at three different MAS rotation frequencies ν_r (15.0, 20.0, and 24.0 kHz) in $MgSiO_3$ glass. As has been noted before [34], one can observe that increasing the spinning frequency leads to an increase in the full width at half height of these partial spectra. Czjzek fittings of the spectra in Fig. 6b also reveal a slight increase in the width of the distribution as a function of the spinning speed, corresponding to a variation of the apparent average quadrupolar coupling constant $\langle|C_Q|\rangle$ from 5.52 MHz at ν_r = 15 kHz to 5.55 MHz at ν_r = 24 kHz. This observation, which at first glance appears counterintuitive, can be explained in terms of the wide distribution of quadrupolar coupling constants that is found in the present samples [34].

The ability of MAS-NMR to provide effective lineshape narrowing depends on the ratio of the spinning frequency to the quadrupolar frequency. On the one hand, the resonance signals of those nuclei affected by strong quadrupolar coupling at the high end of the distribution of C_Q values are unaffected (or little affected) by the MAS sample rotation, contributing to the broad part of the spectrum. On the other hand, the resonance signals of those nuclei that are at the low end of the C_Q distribution (up to a limiting value of C_{Qmax}) show significantly narrowed spectra. The second-order perturbative nature of the interactions still confers a residual anisotropic line broadening effect to the lineshape, which will increase with increasing C_Q value. Increasing the spinning speed will shift the limit of C_{Qmax} towards higher values, which implies that more and more nuclei with higher degrees of distortions in their immediate electronic environments (and hence broader NMR signals) contribute to the narrower feature of the MAS-NMR lineshape. In consequence, this set of nuclei includes more and more nuclei with increasingly distorted environments as the spinning frequency is increased. This effect will always occur if the distribution of quadrupole coupling constants is so wide that only part of the entire ensemble can be detected by MAS-NMR.

Equally important, an absence of a spinning speed dependence of the MAS-NMR spectra on the MAS spinning frequency signifies that all the nuclei present in the sample contribute towards the MAS-narrowed lineshape. In the present case of ^{25}Mg in glasses, our results thus indicate that magnetic field strengths higher than 14.1 T and/or spinning frequencies higher than 24 kHz would be required to reach that situation. Therefore, we suspect that many of the $\langle|C_Q|\rangle$ values for ^{25}Mg reported in the literature for glasses containing magnesium of natural isotopic abundance and measured under similar conditions may be under-estimated. Likewise, the $\langle\delta_{iso}\rangle$ values reported for ^{25}Mg in glasses may not be representative because they only refer to a sub-set of nuclei interacting with weaker EFGs, which contribute to the narrower lineshape feature.

^{25}Mg static spin echo decay spectroscopy

Previous studies have shown that, in principle, Hahn spin echo decay spectroscopy of spin-3/2 and spin-5/2 nuclei can measure the strength of homonuclear magnetic dipole-dipole interactions under conditions of selective excitation of the central $m = ½ \leftrightarrow m = -½$ transition [57,58].

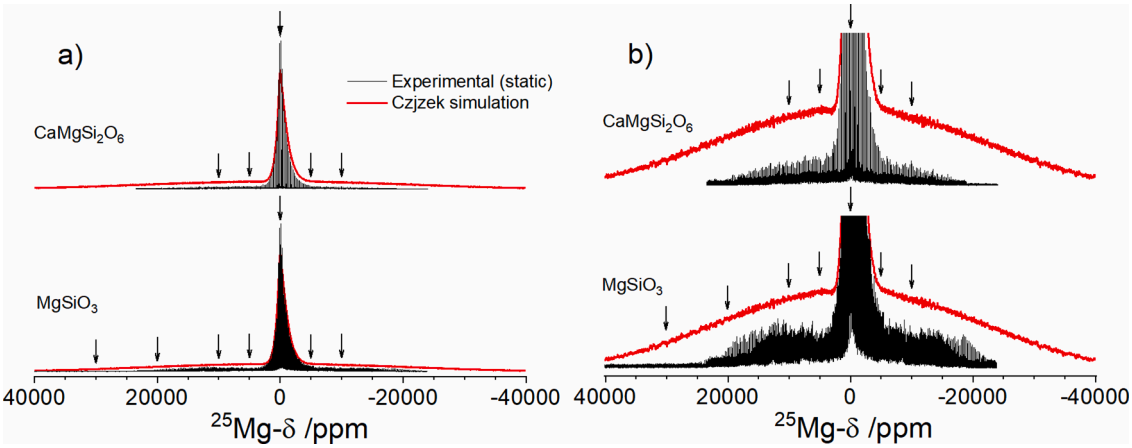

Fig. 4. (a) Full static spectrum for the $MgSiO_3$ and $CaMgSi_2O_6$ glasses, together with simulations using distributions of the EFG that follow the Czjzek model. (b) Vertical expansion emphasizing the quadrupolar satellite spikelets. The arrows indicate the resonance offsets used for the stepwise acquisition of the wideline spectra.

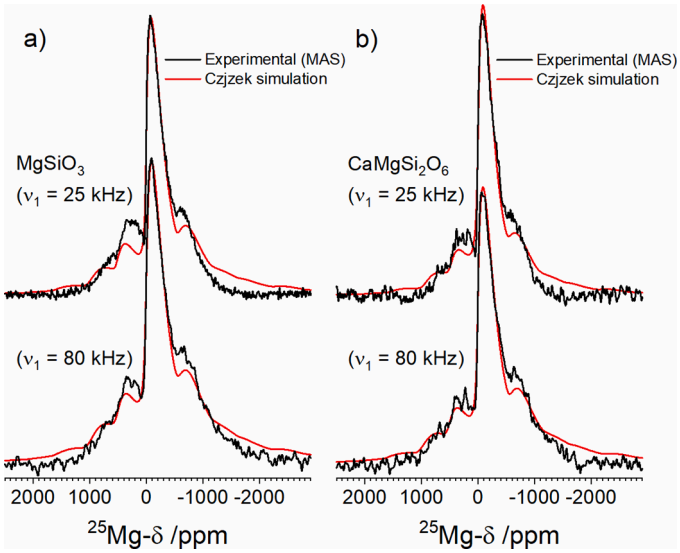

Fig. 5. ^{25}Mg MAS-NMR spectra obtained by rotor-synchronized Hahn-spin echo acquisition at a rotor frequency of 20.0 kHz (acquisition after two rotor cycles – black curves) and simulations considering a distribution of EFGs given by the Czjzek model (red curves) for the (a) $MgSiO_3$ and (b) $CaMgSi_2O_6$ samples. Top: lower radiofrequency power level (non-selective nutation frequency 25 kHz); bottom: higher radiofrequency power level (non-selective nutation frequency 80 kHz).

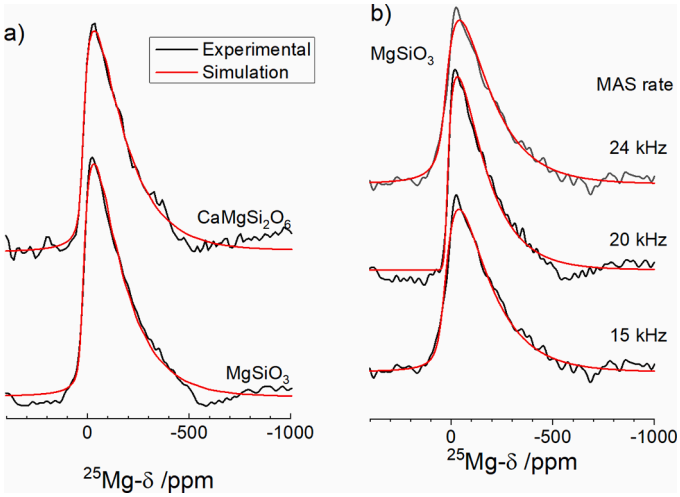

Fig. 6. (a) ^{25}Mg MAS-NMR spectra obtained by rotor-synchronized Hahn-spin echo acquisition at a rotor frequency of 20.0 kHz (acquisition after two rotor cycles), measured at a radio-frequency power corresponding to a non-selective nutation frequency of 25 kHz. The broad feature of Fig. 5 has been eliminated by removing (left shifting) the data acquired within a 24 μs range from the trailing part of the echo prior to Fourier transformation. Red curves show the fit of the remaining lineshape (narrower feature in Fig. 5) to a Czjzek distribution of quadrupolar coupling parameters. (b) Czjzek fits of the spectra following free induction decay (FID) truncation by left shifting the data by 24 μs, effectively eliminating the broad component from the MAS-NMR lineshape measured with ν_r set at 15.0, 20.0 or 24.0 kHz in $MgSiO_3$ glass.

This method has been widely applied to investigate the spatial distribution of sodium ions in oxide glasses [59]. Fig. 7 explores this question with regards to a measurement of the ^{25}Mg-^{25}Mg dipole-dipole interactions in the isotopically enriched materials. Data sets were measured at two distinct nutation frequencies of 25 and 80 kHz. As shown in Fig. 7, the results do not depend on this parameter within the experimental error, indicating that, under both conditions, the central transition is selectively excited.

The results indicate that the spin echo signal of diopside glass decays slightly faster than that of $MgSiO_3$ glass, particularly at shorter evolution times ($2\tau < 2$ ms). This result is counterintuitive, as the total ^{25}Mg concentration in enstatite glass is twice as high as in diopside glass. Most likely, even in the isotopically enriched materials, the dipole-dipole coupling is so weak that the nuclear electric quadrupolar interaction dominates the spin echo decay response. This expectation is confirmed by additional experiments (see Fig. 7, right), indicating that the echo decay rate in the magnetically diluted samples at natural abundance (10% ^{25}Mg) is comparable to that measured for the isotopically enriched material. We therefore conclude that, even in the isotopically enriched materials, the homonuclear interactions are too weak to be measured by the simple spin echo decay method. More sophisticated techniques, e.g., based on double quantum excitation, may have to be employed.

Comparison with diffraction and molecular dynamics results

Table 2 summarizes the current state of the literature on the ^{25}Mg NMR parameters deduced for magnesium containing silicate glasses. The detailed analysis of the static and MAS-NMR spectra done in the present work shows that the quadrupolar interactions in vitreous $MgSiO_3$ and $CaMgSi_2O_6$ are significantly stronger than previously suggested, but confirms the isotropic chemical shifts published earlier. We further note that in our study the high-field approximation is fulfilled, i.e., the ratio of the quadrupole frequency to the Larmor frequency, ν_Q/ν_0 (~ 0.03) is significantly smaller than the value of 0.1 above which the central transition peak maximum would be affected by a low-frequency quadrupolar shift, as noted by Werner-Zwanziger et al. [60]. Thus, for the ^{25}Mg NMR of these glasses measured at 14.1 T, the average isotropic chemical shift information deduced from our analysis is accurate. In view of the above-mentioned correlation between the isotropic chemical shifts and the coordination number in crystalline compounds [34], this result would suggest that the Mg^{2+} ions detected by NMR are predominantly six-coordinated. In striking contrast to this conclusion, the results obtained from conventional neutron and X-ray diffraction experiments show that vitreous $MgSiO_3$ and $CaMgSi_2O_6$ have a broad distribution of nearest-neighbor Mg-O distances with a mean Mg-O coordination number in the range 4.4–4.8 [21,22,61], significantly smaller than the value of six found for their crystalline counterparts. Likewise, more recent molecular dynamics simulations indicate mean Mg-O coordination numbers in the range of 4.7–4.8 with a distribution of four-, five- and six-coordinated Mg^{2+} ions [20,22]. Experiments using neutron diffraction with magnesium isotope substitution, performed on the same samples investigated by NMR in the present work, give a mean Mg-O coordination number of 4.4–4.5 for both materials [21,61].

In view of the large discrepancy between the NMR and the diffraction/molecular dynamics results, we have re-evaluated our simulation approach by performing further simulations of the ^{25}Mg MAS-NMR spectra for glassy $MgSiO_3$ assuming different isotropic chemical shift scenarios. Fig. 8a and b compare the unconstrained fit ($\delta_{iso} = 13$ ppm, see Fig. 5a) with a simulation constraining the isotropic chemical shift value to $\delta_{iso} = 50$ ppm, which is a typical value for four-coordinated Mg. Although the best-fit simulation provides a δ_{iso} value of 13 ppm, the simulation with δ_{iso} fixed at 50 ppm is also very close to representing the experimental data. The difference in chemical shifts is compensated by a slightly wider distribution of EFGs for the simulation with $\delta_{iso} = 50$ ppm (σ of 4.6 MHz against 4.4 MHz obtained for the unconstrained simulation). Based on these results, it should be possible to fit the MAS-NMR lineshape by assuming multiple Mg sites with coordination numbers of four, five or six.

As a proof of concept, we have simulated the ^{25}Mg spectrum for $MgSiO_3$ by considering a 1:1 ratio of two components representing four- and six-coordinated sites with fixed isotropic chemical shifts of 50 and 13 ppm, respectively. Fig. 8c shows the best fit, when σ and the isotropic line-broadening parameter were adjusted but the relative areas of both

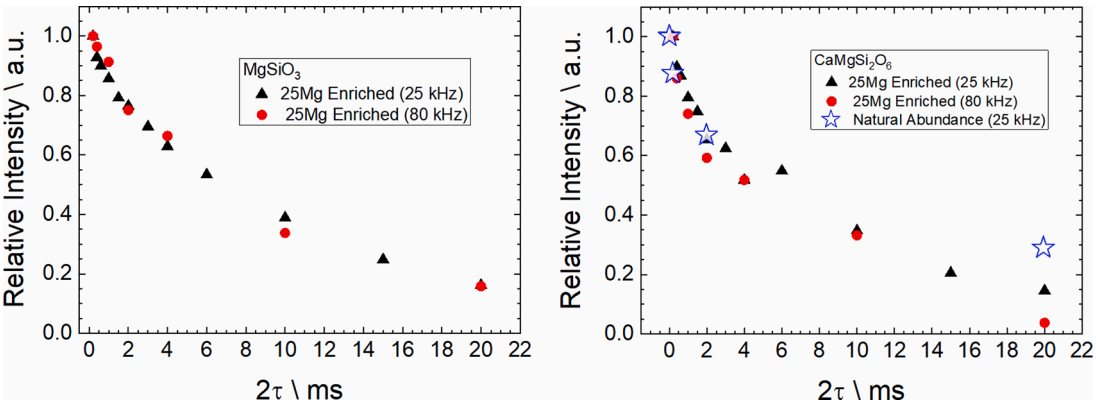

Fig. 7. ^{25}Mg spin echo decay of (left) $MgSiO_3$ glass and (right) $CaMgSi_2O_6$ glass at two radiofrequency power levels, Corresponding to nutation frequencies ν_1 of 25 kHz (black triangles) and 80 kHz (red circles). For the diopside glass, data is also shown for a sample with magnesium of natural isotopic abundance (blue open stars, right).

Table 2
Current state of ^{25}Mg NMR parameters in oxide glasses.

System	$\langle\delta_{iso}\rangle$ (ppm)	$\langle\lvert C_Q\rvert\rangle$ (MHz)	Reference
$MgSiO_3$.Mg_2SiO_4	17	7.6	[15]
$MgSiO_3$	14	2.8	[13]
$MgSiO_3$	13 ± 3	8.6 ± 0.5	This work
$CaMgSi_2O_6$	13 ± 3	8.3 ± 0.5	This work
$CaMgSi_2O_6$	16	2.7	[13]
$Mg_3Al_2Si_3O_{12}$	14	3.2	[13]
$Ca_2MgSi_2O_7$	14	3.9	[13]
$Li_2MgSi_2O_6$	14	2.9	[13]
$Na_2MgSi_2O_6$	41	3.5	[13]
$K_2MgSi_2O_6$	38	2.9	[13,14]
$K_2MgSi_5O_{12}$	37	3.1	[13]
SiO_2-B_2O_3-Al_2O_3-Na_2O-MgO	5–35	6.5–8.5	[25]
SiO_2-B_2O_3-Al_2O_3-Na_2O-MgO†	45–50	–	[62]

† Contains other components such as La_2O_3.

components were kept constant at the 1:1 ratio to represent an average Mg coordination number of five. The simulation in Fig. 8c reinforces our conclusion that, due to the wide distribution of EFGs, the contribution of particular Mg species cannot be quantified and no reliable average Mg coordination number can be deduced from the NMR data alone. In view of the good fit of Fig. 8c, we can certainly consider the ^{25}Mg NMR spectrum to be consistent with the conclusion from the neutron diffraction results [21,61] that enstatite and diopside glasses feature multiple Mg environments in four-, five-, and six-coordination, producing an average coordination number near or somewhat below five.

The triple-quantum MAS (3QMAS) NMR technique is widely employed for quadrupolar nuclei with wide distributions of EFGs due to the possibility of resolving multiple sites in the indirect isotropic dimension. However, this experiment is very challenging for the ^{25}Mg isotope, even for isotopically enriched samples, due to the low frequency and fast transverse relaxation, and typically take measurement times on the order of a few days, even at very high magnetic field strengths. Shimoda et al. have performed 3QMAS experiments at 16.4 and 21.8 T for a variety of Mg-containing glasses, including $MgSiO_3$ and $CaMgSi_2O_6$ [13,14]. For the latter, isotropic shifts of 14-16 ppm suggest that Mg is predominantly six-coordinated. The 3QMAS spectra obtained for enstatite glass at 21.8 T (with a spinning speed of 18 kHz) hint at the presence of four different Mg sites, with isotropic chemical shifts ranging from 1 to 24 ppm [14]. In comparison to our results, the average quadrupolar coupling constants deduced from that work were found to be significantly smaller. Altogether, because of the poor signal-to-noise ratio obtained in those experiments, the possible coexistence of multiple Mg species with different coordination numbers cannot be excluded.

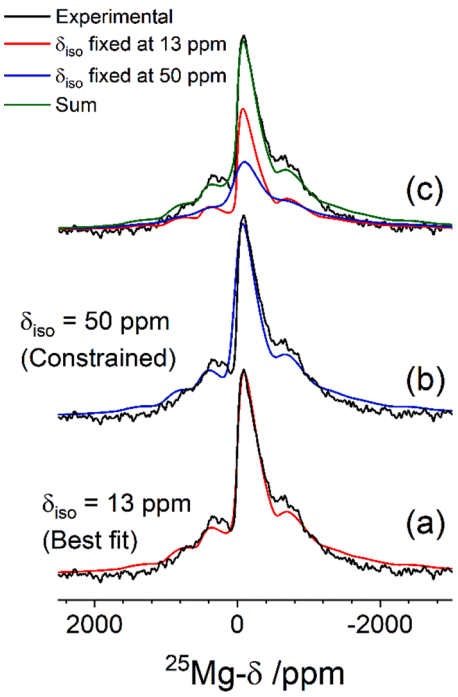

Fig. 8. Comparison of (a) the best-fit unconstrained simulation of the ^{25}Mg MAS-NMR spectrum of glassy $MgSiO_3$ yielding a δ_{iso} value of 13 ppm (also shown in Fig. 5a, ν_1 = 80 kHz) with (b) a constrained simulation, assuming an average δ_{iso} value of 50 ppm mimicking four-coordinated Mg, and (c) a 1:1 superposition of (a) and (b), mimicking an average Mg coordination number of five. All fits include a Gaussian line-broadening parameter of 27 ppm, which accounts for a distribution of isotropic chemical shifts.

We note that other work on alkali magnesium silicate [13] and sodium magnesium aluminoborosilicate glasses has indicated that changes to the average Mg coordination number can be observed by following the trend in the average ^{25}Mg chemical shift with glass composition [25, 62]. We presume that the quadrupolar interactions are weaker and the EFG distributions are narrower than in the present case, but we are planning to re-examine these results in the future using the approach developed in the present paper. For enstatite and diopside glasses, however, we must conclude that solid state NMR may not be a well-suited method for evaluating the average coordination number of the Mg^{2+} ions.

Conclusions

We have presented studies of the static wideline and high-resolution MAS ^{25}Mg NMR lineshapes for enstatite and diopside glasses. Both the static and rotor-synchronized Hahn-echo MAS NMR spectra indicate a broad distribution of the EFG components at the ^{25}Mg position caused by disorder, which can be fitted consistently to a common set of interaction parameters and distribution widths using the Czjzek approach. Our results suggest that the previously published average quadrupolar coupling constants and distribution widths for these glasses may have been underestimated. We estimate average $<|C_Q|>$ values and isotropic chemical shifts of 8–9 MHz and 13 ppm for both the enstatite and diopside glasses. In view of the Mg-O coordination numbers obtained from diffraction experiments and molecular dynamics simulations, this shift does not, however, imply glass structures in which all the Mg^{2+} is six-coordinated. We demonstrate that due to the lack of site-resolution, the NMR data are likely to be well simulated by a superposition of multiple sites with different Mg coordination numbers, consistent with the diffraction data.

The results reported here are of considerable relevance with regards to the spectra of other nuclei with strong quadrupolar interactions and wide distributions of EFGs in glassy materials, as expected for ^{39}K, ^{45}Sc, $^{47/49}$Ti, $^{69/71}$Ga, ^{87}Rb, ^{87}Sr, ^{93}Nb, $^{135/137}$Ba, and ^{139}La. The present paper outlines a general strategy for characterizing the local environments of the corresponding elements in amorphous and glassy materials.

Declaration of Competing Interests

The authors declare that they have no known competing financial interests or personal relationships that could have appeared to influence the work reported in this paper.

Acknowledgments

Funding of this work by FAPESP, Project number 2013/07793–6, is most gratefully acknowledged. M.O.Jr. and H.E. acknowledge the National Council for Scientific and Technological Development (CNPq, grants n° 311069/2020–7 and 310870/2020–8, respectively). H.D. is grateful for personal fellowship support from CNPq and Nippon Electric Glass. P.S.S. received support from the University of Bath's International Funding Scheme. We thank Laurent Cormier (Paris) for providing the samples and Hesameddin Mohammadi and Rita Mendes da Silva (Bath) for access to their diffraction results prior to publication.

References

[1] D.J. Backhouse, C.L. Corkhill, N.C. Hyatt, R.J. Hand, Investigation of the role of Mg and Ca in the structure and durability of aluminoborosilicate glass, J. Non. Cryst. Solids. 512 (2019) 41–52.
[2] M. Lograd, H. Eckert, T. Murata, S. Nakane, H. Yamazaki, Structure-property relations in crack-resistant alkaline-earth aluminoborosilicate glasses studied by solid state NMR, J. Am. Ceram. Soc. 104 (2021) 2250–2267.
[3] H. Bradtmüller, T. Uesbeck, H. Eckert, T. Murata, S. Nakane, H. Yamazaki, Structural origins of crack resistance on magnesium aluminoborosilicate glasses studied by solid-state NMR, J. Phys. Chem. C. 123 (2019) 14941–14954.
[4] X. Zhang, Y. Yue, H. Wu, Effects of MgO/CaO on the structural, thermal and dielectric properties of aluminoborosilicate glasses, J. Mater. Sci. Mater. Electron. 24 (2013) 2755–2760.
[5] M.T. Souza, M.C. Crovace, C. Schröder, H. Eckert, O. Peitl, E.D. Zanotto, Effect of magnesium ion incorporation on the thermal stability, dissolution behavior and bioactivity in bioglass-derived glasses, J. Non. Cryst. Solids. 382 (2013) 57–65.
[6] S.J. Watts, R.G. Hill, M.D. O'Donnell, R.V. Law, Influence of magnesia on the structure and properties of bioactive glasses, J. Non. Cryst. Solids. 356 (2010) 517–524.
[7] H. Aguiar, E.L. Solla, J. Serra, P. González, B. León, F. Malz, C. Jäger, Raman and NMR study of bioactive Na_2O–MgO–CaO–P_2O_5–SiO_2 glasses, J. Non. Cryst. Solids. 354 (2008) 5004–5008.
[8] J.M. Oliveira, R.N. Correia, M.H. Fernandes, J. Rocha, Influence of the CaO/MgO ratio on the structure of phase-separated glasses: a solid state ^{29}Si and ^{31}P MAS NMR study, J. Non. Cryst. Solids. 265 (2000) 221–229.
[9] Y. Tabira, Local structure around oxygen atoms in $CaMgSi_2O_6$ glass by O K-edge EXELFS, Mater. Sci. Eng. B. 41 (1996) 63–66.
[10] M.C. Wilding, C.J. Benmore, J.A. Tangeman, S. Sampath, Evidence of different structures in magnesium silicate liquids: coordination changes in forsterite- to enstatite-composition glasses, Chem. Geol. 213 (2004) 281–291.
[11] P. Ildefonse, G. Calas, A.M. Flank, P. Lagarde, Low Z elements (Mg, Al, and Si) K-edge X-ray absorption spectroscopy in minerals and disordered systems, Nucl. Instrum. Methods Phys. Res. Sect. B Beam Interact. Mater. Atoms. 97 (1995) 172–175.
[12] L. Dien, P. Mingsheng, T. Murata, Coordination and local structure of magnesium in silicate minerals and glasses; Mg K-edge XANES study, Can. Mineral. 37 (1999) 199–206.
[13] K. Shimoda, T. Nemoto, K. Saito, Local structure of magnesium in silicate glasses: a ^{25}Mg 3QMAS NMR study, J. Phys. Chem. B. 112 (2008) 6747–6752.
[14] K. Shimoda, Y. Tobu, M. Hatakeyama, T. Nemoto, K. Saito, Structural investigation of Mg local environments in silicate glasses by ultra-high field ^{25}Mg 3QMAS NMR spectroscopy, Am. Mineral. 92 (2007) 695–698.
[15] S. Sen, H. Maekawa, G.N. Papatheodorou, Short-range structure of invert glasses along the pseudo-binary join $MgSiO_3$-Mg_2SiO_4: results from ^{29}Si and ^{25}Mg MAS NMR spectroscopy, J. Phys. Chem. B. 113 (2009) 15243–15248.
[16] T.T. Nguyen, T.T. Nguyen, H.T. Dinh, V.V. Le, Molecular dynamics simulations of structural and mechanical properties in $MgSiO_3$ Glass, Phys. Status Solidi. 256 (2019), 1900215.
[17] T. Taniguchi, M. Okuno, T. Matsumoto, X-ray diffraction and EXAFS studies of silicate glasses containing Mg, Ca and Ba atoms, J. Non. Cryst. Solids. 211 (1997) 56–63.
[18] J.D. Kubicki, A.C. Lasaga, Molecular dynamics simulations of pressure and temperature effects on $MgSiO_3$ and Mg_2SiO_4 melts and glasses, Phys. Chem. Miner. 17 (1991) 661–673, https://doi.org/10.1007/BF00202236.
[19] K. Shimoda, M. Okuno, Molecular dynamics study of $CaSiO_3$ –$MgSiO_3$ glasses under high pressure, J. Phys. Condens. Matter. 18 (2006) 6531–6544.
[20] D.B. Ghosh, B.B. Karki, L. Stixrude, First-principles molecular dynamics simulations of $MgSiO_3$ glass: structure, density, and elasticity at high pressure, Am. Mineral. 99 (2014) 1304–1314.
[21] L. Cormier, G.J. Cuello, Mg coordination in a $MgSiO_3$ glass using neutron diffraction coupled with isotopic substitution, Phys. Rev. B. 83 (2011), 224204.
[22] P.S. Salmon, G.S. Moody, Y. Ishii, K.J. Pizzey, A. Polidori, M. Salanne, A. Zeidler, M. Buscemi, H.E. Fischer, C.L. Bull, S. Klotz, R. Weber, C.J. Benmore, S. G. MacLeod, Pressure induced structural transformations in amorphous $MgSiO_3$ and $CaSiO_3$, J. Non-Cryst. Solids X. 3 (2019), 100024.
[23] S. Kroeker, J.F. Stebbins, Magnesium coordination environments in glasses and minerals: new insight from high-field magnesium-25 MAS NMR, Am. Mineral. 85 (2000) 1459–1464.
[24] S. Kroeker, P.S. Neuhoff, J.F. Stebbins, Enhanced resolution and quantitation from `ultrahigh' field NMR spectroscopy of glasses, J. Non. Cryst. Solids. 293–295 (2001) 440–445.
[25] N. Bisbrouck, M. Bertani, F. Angeli, T. Charpentier, D. Ligny, J. Delaye, S. Gin, M. Micoulaut, Impact of magnesium on the structure of aluminoborosilicate glasses: a solid-state NMR and Raman spectroscopy study, J. Am. Ceram. Soc. 104 (2021) 4518–4536.
[26] B. Zhou, A. Faucher, R. Laskowski, V.V. Terskikh, S. Kroeker, W. Sun, J. Lin, J.-. X. Mi, V.K. Michaelis, Y. Pan, Ultrahigh-Field ^{25}Mg NMR and DFT study of magnesium borate minerals, ACS Earth Space Chem. 1 (2017) 299–309.
[27] P.J. Pallister, I.L. Moudrakovski, J.A. Ripmeester, Mg-25 ultra-high field solid state NMR spectroscopy and first principles calculations of magnesium compounds, Phys. Chem. Chem. Phys. 11 (2009) 11487–11500.
[28] M. Hatakeyama, T. Nemoto, K. Kanehashi, K. Saito, Natural abundance solid-state ^{25}Mg MQMAS NMR studies on inorganic solids at a high magnetic field of 16.4 T, Chem. Lett. 34 (2005) 864–865.
[29] J.M. Griffin, A.J. Berry, S.E. Ashbrook, Observation of "hidden" magnesium: first-principles calculations and ^{25}Mg solid-state NMR of enstatite, Solid State Nucl. Magn. Reson. 40 (2011) 91–99.
[30] N.G. Dowell, S.E. Ashbrook, S. Wimperis, Satellite-transition MAS NMR of low-γ nuclei at natural abundance: sensitivity, practical implementation, and application to ^{39}K (I = 3/2) and ^{25}Mg (I = 5/2), J. Phys. Chem. B. 108 (2004) 13292–13299, https://doi.org/10.1021/jp047868m.
[31] F.H. Larsen, J. Skibsted, H.J. Jakobsen, N.C. Nielsen, Solid-state QCPMG NMR of low-γ quadrupolar metal nuclei in natural abundance, J. Am. Chem. Soc. 122 (2000) 7080–7086, https://doi.org/10.1021/ja0003526.
[32] L.S. Cahill, J.V. Hanna, A. Wong, J.C.C. Freitas, J.R. Yates, R.K. Harris, M.E. Smith, Natural abundance ^{25}Mg solid-state NMR of Mg oxyanion systems: a combined experimental and computational study, Chem. Eur. J. 15 (2009) 9785–9798.
[33] D. Laurencin, C. Gervais, H. Stork, S. Krämer, D. Massiot, F. Fayon, ^{25}Mg solid-state NMR of magnesium phosphates: high magnetic field experiments and density functional theory calculations, J. Phys. Chem. C. 116 (2012) 19984–19995.
[34] J.C.C. Freitas, M.E. Smith, Recent advances in solid-state ^{25}Mg NMR spectroscopy, Annu. Rep. NMR Spectrosc. 75 (2012) 25–114.
[35] I.L. Moudrakovski, Recent advances in solid-state NMR of alkaline earth elements, Annu. Rep. NMR Spectrosc. 79 (2013) 129–240.
[36] V.R. Seymour, S.P. Day, G. Scholz, K. Scheurell, D. Iuga, J.M. Griffin, E. Kemnitz, J. V. Hanna, M.E. Smith, A Combined ^{25}Mg solid-state NMR and ab initio DFT approach to probe the local structural differences in magnesium acetate phases Mg $(CH_3COO)_2{\cdot}nH_2O$ (n = 0, 1, 4), Chem. Phys. Chem. 19 (2018) 1722–1732.
[37] A.M. George, J.F. Stebbins, Structure and dynamics of magnesium in silicate melts; a high-temperature ^{25}Mg NMR study, Am. Mineral. 83 (1998) 1022–1029.
[38] L. Cormier, G.J. Cuello, Structural investigation of glasses along the $MgSiO_3$–$CaSiO_3$ join: diffraction studies, Geochim. Cosmochim. Acta. 122 (2013) 498–510.

[39] E. Kupce, R. Freeman, Adiabatic pulses for wideband inversion and broadband decoupling, J. Magn. Reson. Ser. A. 115 (1995) 273–276.
[40] R. Bhattacharyya, L. Frydman, Quadrupolar nuclear magnetic resonance spectroscopy in solids using frequency-swept echoing pulses, J. Chem. Phys. 127 (2007), 194503.
[41] L.A. O'Dell, R.W. Schurko, QCPMG using adiabatic pulses for faster acquisition of ultra-wideline NMR spectra, Chem. Phys. Lett. 464 (2008) 97–102.
[42] L.A. O'Dell, A.J. Rossini, R.W. Schurko, Acquisition of ultra-wideline NMR spectra from quadrupolar nuclei by frequency stepped WURST–QCPMG, Chem. Phys. Lett. 468 (2009) 330–335.
[43] R.W. Schurko, Ultra-wideline solid-state NMR spectroscopy, Acc. Chem. Res. 46 (2013) 1985–1995.
[44] L.A. O'Dell, The WURST kind of pulses in solid-state NMR, Solid State Nucl. Magn. Reson. 55–56 (2013) 28–41.
[45] H.Y. Carr, E.M. Purcell, Effects of diffusion on free precession in nuclear magnetic resonance experiments, Phys. Rev. 94 (1954) 630–638, https://doi.org/10.1103/PhysRev.94.630.
[46] S. Meiboom, D. Gill, Modified spin-echo method for measuring nuclear relaxation times, Rev. Sci. Instrum. 29 (1958) 688–691.
[47] S.G.J. van Meerten, W.M.J. Franssen, A.P.M. Kentgens, ssNake: a cross-platform open-source NMR data processing and fitting application, J. Magn. Reson. 301 (2019) 56–66.
[48] M. Bak, J.T. Rasmussen, N.C. Nielsen, SIMPSON: a general simulation program for solid-state NMR spectroscopy, J. Magn. Reson. 147 (2000) 296–330.
[49] J. Schneider, V.R. Mastelaro, E.D. Zanotto, B.A. Shakhmatkin, N.M. Vedishcheva, A.C. Wright, H. Panepucci, Q^n distribution in stoichiometric silicate glasses: thermodynamic calculations and ^{29}Si high-resolution NMR measurements, J. Non. Cryst. Solids. 325 (2003) 164–178.
[50] S.J. Gaudio, S. Sen, C.E. Lesher, Pressure-induced structural changes and densification of vitreous $MgSiO_3$, Geochim. Cosmochim. Acta 72 (2008) 1222–1230.
[51] J. Schneider, V.R. Mastelaro, H. Panepucci, E.D. Zanotto, ^{29}Si MAS–NMR studies of Q^n structural units in metasilicate glasses and their nucleating ability, J. Non. Cryst. Solids 273 (2000) 8–18.
[52] D.G. Fraser, N.J. Clayden, A high-resolution ^{29}Si nuclear magnetic resonance study of ordering in silicate glasses on the join $CaMgSi_2O_6$ - $NaAlSi_3O_8$, Chem. Geol. 62 (1987) 43–47.
[53] G. Libourel, C.A. Geiger, L. Merwin, A. Sebald, ^{29}Si and ^{27}Al MAS-NMR spectroscopy of glasses in the system $CaSiO_3$-$MgSiO_3$-Al_2O_3, Chem. Geol. 96 (1992) 387–397.
[54] J.-B. d'Espinose de Lacaillerie, C. Fretigny, D. Massiot, MAS NMR spectra of quadrupolar nuclei in disordered solids: the Czjzek model, J. Magn. Reson. 192 (2008) 244–251.
[55] G. Czjzek, J. Fink, F. Götz, H. Schmidt, J.M.D. Coey, J.-P. Rebouillat, A. Liénard, Atomic coordination and the distribution of electric field gradients in amorphous solids, Phys. Rev. B. 23 (1981) 2513–2530, https://doi.org/10.1103/PhysRevB.23.2513.
[56] M. Edén, Computer simulations in solid-state NMR. III. Powder averaging, Concepts Magn. Reson. Part A Bridg. Educ. Res. 18 (2003) 24–55, https://doi.org/10.1002/cmr.a.10065.
[57] B. Gee, H. Eckert, ^{23}Na nuclear magnetic resonance spin echo decay spectroscopy of sodium silicate glasses and crystalline model compounds, Solid State Nucl. Magn. Reson. 5 (1995) 113–122.
[58] J. Haase, E. Oldfield, Spin-echo behavior of nonintegral-spin quadrupolar nuclei in inorganic solids, J. Magn. Reson. Ser. A. 101 (1993) 30–40.
[59] H. Eckert, Short and medium range order in ion-conducting glasses studied by modern solid state NMR techniques, Z. Phys. Chem. 224 (2010) 1591–1654.
[60] U. Werner-Zwanziger, A.L. Paterson, J.W. Zwanziger, The Czjzek distribution in solid-state NMR: scaling properties of central and satellite transitions, J. Non. Cryst. Solids. 550 (2020), 120383.
[61] R. Mendes Da Silva, H. Mohammadi, (private communication).
[62] R. Guo, C.T. Brigden, S. Gin, S.W. Swanton, I. Farnan, The effect of magnesium on the local structure and initial dissolution rate of simplified UK Magnox waste glasses, J. Non. Cryst. Solids. 497 (2018) 82–92.